Received: 18 December 2023 | Revised: 27 June 2024 | Accepted: 13 August 2024

DOI: 10.1002/jex2.70006

RESEARCH ARTICLE

Shining a light on fluorescent EV dyes: Evaluating efficacy, specificity and suitability by nano-flow cytometry

Joseph Brealey[1] | **Rebecca Lees**[1] | **Robert Tempest**[1] | **Alice Law**[1] | **Sonia Guarnerio**[2] | **Rawan Maani**[2] | **Soozana Puvanenthiran**[3] | **Nick Peake**[2] | **Ryan Pink**[3] | **Ben Peacock**[1]

[1]NanoFCM Co., Ltd., Nottingham, UK

[2]Sheffield Hallam University, Biomolecular Sciences Research Centre, Sheffield, UK

[3]Faculty of Health and Life Sciences, Oxford Brookes University, Oxford, UK

Correspondence
Ben Peacock, NanoFCM Co., Ltd., Nottingham, UK. Email: Bpeacock@nanoFCM.com

Abstract

Extracellular vesicles (EVs) are mediators of intercellular communication, recently recognised for their clinical applications. Accurate characterisation and quantification of EVs are critical for understanding of their function and clinical relevance. Many platforms utilise fluorescence for EV characterisation, frequently labelling surface proteins to identify EVs. The heterogeneity of EVs and the lack of a universal protein marker encourages the use of generic EV labelling methods, including membrane labelling. Using nano-flow cytometry, we evaluated six membrane dyes, including MemGlow and CellMask. Evaluation criteria included EV labelling efficacy, non-specific labelling of very low-density lipoproteins (VLDLs), brightness and dye aggregation. Significant variation was observed in dye performance, with certain dyes showing poor EV labelling efficacy or high affinity to VLDLs. Importantly, several promising candidates were identified for further investigation. Overall, this study highlights the importance of selecting appropriate membrane dyes for EV staining tailored to the aims of the study and the EV origin. MemGlow and CellMask proved favourable, allowing bright, sensitive staining of EV membranes with minimal aggregation. However, MemGlow showed an affinity to VLDLs, and CellMask requires additional sample handling for optimal labelling. These results contribute to deepening our understanding of EV membrane dyes, allowing for better dye selection and EV identification in future studies.

KEYWORDS

brightness, extracellular vesicles (EVs), fluorescent labelling, membrane dyes, nano-flow cytometry, single particle characterisation, specificity

1 | INTRODUCTION

Extracellular vesicles (EVs) are small membranous particles released by cells into their surrounding environment, including the intercellular space, local tissue stroma, bloodstream, saliva, urine and other bodily fluids (Kalluri & LeBleu, 2020). EVs are important mediators of cell-to-cell communication and signalling, and research into the functions and properties of EVs has revealed their critical roles in physiological and pathological processes such as inflammation, immune regulation, cancer metastasis and neurodegenerative diseases (Buzas, 2023; Chang et al., 2021; Yates et al., 2022). Moreover, EVs have emerged as promising tools for diagnostics and therapeutics due to their ability to carry bioactive molecules and deliver them to specific target cells (Gurunathan et al., 2021). This study will focus on small EVs (sEVs) <200 nm, recognising that many common isolation techniques do not aim to distinguish between EVs of different sub-types or biogenesis routes.

In recent years, numerous techniques have been used to characterise and detect EVs, including electron microscopy (EM), nanoparticle tracking analysis (NTA), flow cytometry (including conventional, high-resolution and nano-flow cytometry), western blotting (WB), mass spectrometry and microscopy (Bağcı et al., 2022; De Sousa et al., 2023; Kwon & Park, 2022). In combination, these methods allow for the determination of EV size, morphology, protein and lipid composition and nucleic acid content (Théry et al., 2018). However, each method has its advantages and limitations, and selecting the appropriate combination of techniques depends on the research question and sample type.

The evolution of EV analytical techniques has progressed from bulk analyses to single particle analyses, allowing for enhanced particle quantification which distinguishes EV subpopulations from within complex heterogeneous samples (Couch et al., 2021; Dehghani & Gaborski, 2020). Many of these techniques can utilise fluorescent labelling to either characterise EV subpopulations with unique properties and cargo or detect and quantify EVs from other particles within a sample.

Antibody labelling of common EV markers is a well-used strategy for EV detection using many platforms. However, currently, there are no protein targets for antibody labelling that are presented on the surface of a majority of EVs in sufficient quantities to yield successful labelling and detection across all platforms (Kowal et al., 2016).

The heterogeneity of EVs, even within distinct subtypes such as exosomes, means that not every EV will express all common EV markers (Matsui et al., 2021). It has been demonstrated that some EV populations from both cell culture and biofluid samples are negative for the tetraspanins CD9 and CD63 (Laulagnier et al., 2018). Even when key tetraspanins are found in high quantities by bulk analyses, their uneven distribution at a single particle level can introduce sensitivity bias across multiple platforms (Mizenko et al., 2021). These tetraspanins may be less essential to EV biogenesis than originally thought, with some studies revealing that CD9 and CD63 may play only limited roles in several core EV functions, such as cell uptake and cargo delivery (Tognoli et al., 2023). Additionally, recent mass spectrometry data has demonstrated that EVs lacking these "core" EV proteins present similar protein compositions to other EV cohorts (Fan et al., 2023).

With this in mind, numerous lipophilic and membrane-permeable dyes have been utilised to achieve generic EV labelling (Colombo et al., 2021) without relying on protein markers like CD9, CD63 or CD81. Importantly, however, colocalization experiments have suggested that even when an EV protein marker is present, some common dyes are not able to bind the same EV (Melling et al., 2022). This highlights the importance of thoroughly investigating available membrane dyes to determine which are suitable for generic EV labelling.

1.1 | Labelling mechanisms of action

While few dyes are created with EVs in mind, multiple mechanisms of action have been proposed for dye labelling of membranes. Several dyes have been developed which integrate directly into the lipid bilayer. These include the proprietary lipid-mimicking probes MemGlow (Collot et al., 2019) and Cell Mask Deep Red (CMDR).

The ExoBrite family of dyes are fluorescent conjugates of cholera toxin subunit B (CTB), which binds with high affinity to the GM1 ganglioside on mammalian cells and EVs (Baldauf et al., 2015). Reliance on a specific marker gives ExoBrite dyes the same drawbacks as antibody labelling, primarily that marker expression may be heterogeneous between EV sources and within EV populations.

An altogether different mechanism of EV staining is utilised by CellTracker Deep Red (CTDR). CTDR is similar in mechanism to the dye carboxyfluorescein succinimidyl ester (CFSE) (Chuo et al., 2018), in which a non-fluorescent, membrane-permeable molecule enters EVs and covalently binds to lysine residues of internal proteins through its succinimidyl group (Quah & Parish, 2010). Hydrolysis of acetyl groups by EV-internal esterase enzymes activates fluorescence and renders the molecule less membrane permeable (Banks et al., 2013). Therefore, fluorescence with CTDR indicates not only the presence of a membrane but also the presence of active esterase enzymes.

1.2 | Parameters for dye assessment

Paramount to a successful fluorescent EV label is the ability to bind all available EVs and make them detectable by most fluorescence methods. In practice, the evaluation of this must consider the set-up and resolution of the detection instrument as well as the brightness of the labelled EV. In this study, EVs isolated from cell-conditioned media by size exclusion chromatography (SEC) were the primary target for the panel of dyes, as EVs are expected to make up the majority of isolated particles (Contreras et al., 2023). The detection method was nano-flow cytometry, providing high resolution for both labelled and unlabelled EV samples, allowing for thorough analysis of EV labelling with each dye (Tian et al., 2018; Zhu et al., 2014).

Non-specific labelling of common particle co-isolates is an important consideration, especially when working with biofluid-derived EVs. A major non-EV co-isolate is lipoproteins, although the type differs by isolation method (Koster et al., 2021). In particular, when utilising density-based isolation techniques like ultracentrifugation (UC), high-density lipoproteins (HDLs)

TABLE 1 The manufacturer, peak excitation and emission and stock and optimum concentrations of each of the 6 dyes investigated.

Dye	Manufacturer and product code	Excitation/emission (nm)	Stock concentration	Optimum concentration (dilution from stock)
Memglow 488	Cytoskeleton, Inc. MG01	499 / 507	40 μM	40 nM (1:1k)
MemGlow 640	Cytoskeleton, Inc. MG04	650 / 673	40 μM	40 nM (1:1k)
ExoBrite 490/515	Biotium 30112	490 / 516	500×	10× (1:50)
ExoBrite 640/660	Biotium 30114	642 / 663	500×	10× (1:50)*
CellTracker Deep Red (CTDR)	ThermoFisher C34565	630 / 650	1 mM	500 nM (1:2k)*
CellMask Deep Red (CMDR)	ThermoFisher C10046	649 / 666	5 mg/mL	1.25 μg/mL (1:4k)*

Note: Optimum concentration is the best concentration for staining 2×10^{10} particles/mL, as determined by dilution series using nFCM. Concentration units match those given in the product information from the manufacturers. Colours correspond to fluorescent channels used to detect fluorescence: Green = 525/40 nm bandpass filter, red = 670/30 nm. Concentrations marked with an asterisk (*) had to be decreased for staining of plasma particles, due to high fluorescent background. Concentrations used were 2× (ExoBrite 640/660), 62.5 nM (CTDR), and 78.1 ng/mL (CMDR).

and low-density lipoproteins (LDLs) may co-isolate with EVs. When utilising size-based isolation techniques like SEC, very low-density lipoproteins (VLDLs) and chylomicrons may co-isolate with EVs (Brennan et al., 2020). Identifying EVs or EV subpopulations within a complex particle mixture is crucial for the assessment of sample purity. To achieve this, membrane dyes must label EVs without non-specifically labelling other lipid-based structures like lipoproteins.

It's possible for dyes to aggregate or form micelle structures of similar size to EVs, particularly if they contain long hydrocarbon chains that increase hydrophobicity (Pužar Dominkuš et al., 2018). This can interfere with both quantification of EVs and further studies, including EV uptake or internalisation experiments, which investigate the effect of endogenous EVs on recipient cells by tracking their internalisation and localisation in cell cultures (Durak-Kozica et al., 2018) and in vivo and ex vivo experiments (Sun et al., 2019). False (non-EV) particles, either formed or mislabelled by the fluorescent dye, should be identified earlier to avoid data misinterpretation. This is a well-known concern when using PKH67, a commonly used lipophilic dye which inserts an aliphatic chain into the lipid bilayer of EVs, yet also self-aggregates to form micelles of similar size to EVs (Chen et al., 2023; Lai et al., 2015).

Finally, the brightness that each dye can provide for an EV is highly relevant. Brightly labelled EVs allow for the detection of smaller EVs on less sensitive instruments, improving the ability to detect and measure the full range of EVs in a sample. Providing data for the brightness of a given EV dye is surprisingly complex. The fluorescent molecule is often not disclosed and varies between dyes, complicating the use of reference materials like MESF beads for unit conversion to non-arbitrary units.

In addition, when discussing brightness, it is important to consider the optical specifications of the instrument. Using the NanoFCM NanoAnalyzer, the primary instrument in this study, green dyes are excited by the 488 nm blue laser, while emission is measured by a detector behind a 525/40 nm bandpass filter. Red dyes are excited by the 638 nm red laser, while emission is measured by a detector behind a 670/30 nm bandpass filter. Dyes were chosen such that their excitation and emission spectra (Table 1) match the NanoAnalyzer specifications as well as possible, but other optical set-ups could allow for improved detection of some dyes.

To encompass the complexities of describing dye brightness, the stain index of particles labelled with each dye was calculated. The stain index represents the difference in fluorescence intensity between the stained and unstained particles, taking into consideration both the brightness of stained particles and the fluorescent background (Maecker et al., 2004).

In this study, we assess the performance of six commercially available fluorescent EV membrane dyes, with the aim of identifying a dye which brightly labels EVs with high efficacy and specificity. Additionally, by assessing aggregate formation, we determine which dyes may confound assays by presenting false signals similar to EVs. A thoroughly characterised fluorescent dye satisfying the outlined criteria would be a valuable tool for researchers, providing another method of EV identification independent of heterogeneously expressed EV markers like CD9/63/81. Because of its high fluorescence sensitivity and ability to detect unlabelled particles by side-scatter, we will utilise nano-flow cytometry (NanoAnalyzer, NanoFCM) to investigate these dyes.

2 | MATERIALS AND METHODS

2.1 | Preparation and storage of EVs—cell culture + isolation

2.1.1 | EVs from cell-conditioned medium

SW480 and SW620 cell lines were obtained from the European Collection of Cell Culture (Salisbury, UK) and were cultured in complete medium (DMEM (high glucose 4.5 g/L) with 10% FBS and 1% penicillin/streptomycin) and passaged at a confluence of 70%−90%. For seeding into bioreactors, the passage number did not exceed 5, and cell viability was >95%.

To ensure EVs from the FBS used in standard complete mediums did not contaminate any EV collections, EV-depleted medium was required for certain stages of experiments. This was prepared by ultrafiltration of FBS using Amicon Ultra-15 centrifugal filters (MWCO = 100 kDa; Merck Millipore Ltd.) for 55 min at 3000 × *g*, followed by filter sterilisation using a 0.22 μm filter (Kornilov et al., 2018).

The bioreactor (Integra CELLine AD1000) membrane was equilibrated by adding 50 mL complete medium to the outer compartment and incubating for 5 min at 37°C. Approximately 25×10^6 viable cells in the log growth phase were suspended in 15 mL fresh medium and dispensed into the inner compartment using a syringe and blunt-end needle. After seeding, 450 mL of complete medium was added to the outer compartment before sealing all ports and incubating at 37°C with 5% CO_2. The bioreactor was left for 10 days for cells to establish within the inner compartment matrix. Outer compartment media was then discarded and replaced with 500 mL of fresh complete media, with the FBS concentration reduced from 10% to 5% for the remainder of the bioreactor's operation. Medium from the inner compartment was carefully aspirated by a syringe and needle and discarded. Cells were washed three times with PBS, and then 15 mL of EV-depleted media was added to the inner compartment. From this point, 15 mL of EV-rich, cell-conditioned medium could then be harvested every 7 days from the inner compartment, cells washed three times with PBS, and both compartments refreshed with the new medium. Collections were cleared of cells and cellular debris by centrifugation for 10 min at 300 × *g*, followed by 10 min at 2000 × *g*, before storing at −80°C where necessary. Bioreactors were kept for up to 2 months from the point of cell seeding. Conditioned media was concentrated to 0.5 mL using Vivaspin 20 ultrafiltration units (MWCO = 100 kDa; Sartorius) at 3000 × *g* prior to SEC.

SEC Columns were prepared using Econo-Pac chromatography columns (Bio-Rad) and Sepharose CL-2B (Cytiva). The column was stacked with 14 mL Sepharose and topped up to 20 mL with PBS before being left to settle overnight at room temperature, resulting in a resin bed volume of 10 mL. A fret was carefully placed above the resin bed to avoid disturbing the column, before washing three times with 20 mL PBS. 0.5 mL sample was added to the column, followed by 10 mL of PBS, and then 20 × 0.5 mL fractions were collected.

The protein concentration of each SEC fraction was determined by BCA assay (ThermoFisher, 23225, Figure S1a), and the particle concentration was measured by nFCM. Particle-containing fractions were pooled.

2.1.2 | Particles from human plasma

Blood was taken from a healthy volunteer under Oxford Brookes University Ethics Board approval. Venepuncture was carried out at 8 a.m. before food intake into EDTA vacutainer tube by cannulation needle. Within 3 h, the blood was centrifuged for 10 min at 1000 × *g* to collect the plasma. The plasma was diluted with an equal volume of PBS and centrifuged for 15 min at 1500 × *g*. The supernatant was centrifuged for 15 min at 2500 × *g*. The supernatant was then centrifuged at 16,000 × *g* for 35 min, then the supernatant was stored at −80°C until further use.

For SEC, 14 mL SEC columns (BioRad) were filled with 14 mL CL-2B Sepharose slurry and topped up with sterile PBS. Sepharose was allowed to settle for 4 h and bed support was added. Columns were washed through with 10 mL PBS three times and used immediately. 0.5 mL PDP was thawed at 4°C and pipetted above the column bed support. The column was topped up with 10 mL sterile PBS, 2.5 mL of flow-through was collected from the column and discarded, and 1.5 mL flow-through was then collected into a fresh non-stick tube as EVs and stored at 4°C.

2.2 | VLDLs

To assess the specificity of the dyes to non-membranous lipid structures, VLDLs (Lee BioSolutions, 365-10) were purchased. Particle concentrations (>40 nm) were determined by nFCM, then VLDLs were treated identically to EVs.

2.2.1 | EV storage

After isolation, EVs in PBS were split into 25−50 μL aliquots and stored at −80°C. Aliquots were defrosted immediately before use and were subsequently stored in PBS at 4°C for no longer than 7 days. Once defrosted, aliquots were not re-frozen.

2.2.2 | EV characterisation

Prior to use, the size and concentration of SW620-derived and SW480-derived EVs were measured by nFCM (Figure S1b). In addition, both EV samples were stained for CD9, CD63 and CD81, both individually and as a cocktail (Abcam—FITC CD9 (ab18241), CD63 (ab18235), CD81 (ab239256)) (Figure S1c). EVs were incubated with antibodies following the staining protocol below. To allow optimal fluorescent detection (Lees et al., 2022), the antibodies were diluted 30-fold (FITC) for incubation with EVs.

Both EV samples were probed for several EV-associated proteins by western blotting (Figure S1d). Briefly, the EV samples, along with cell lysate, were lysed in Laemmli sample buffer, heated for 2 min at 95°C, and then separated on 4%−20% gradient SDS-PAGE gels (Bio-Rad, Watford, UK) by electrophoresis and transferred to PVDF membranes using preassembled transfer stacks on the trans-blot turbo system (Bio-Rad). Membranes were blocked with 5% non-fat milk and then incubated with primary antibodies to CD9, CD63, TSG101 and GM130 (Abcam, Cambridge, UK). Markers were detected using HRP-conjugated secondary antibodies (Abcam, Cambridge, UK) followed by exposure to SuperSignal West Femto ECL reagent (Thermo-Fisher) and visualised on an Odyssey Li-Cor system (Li-cor, USA).

Finally, the EV samples were observed by TEM (Figure S1e). Briefly, EVs were adsorbed onto carbon-coated copper grids for 1 min, excess fluid was removed by filter paper, and negative staining was performed by placing grids sequentially into 2 drops of water and then 20 μL of filtered 2% uranyl acetate for 2 min. Excess liquid was removed and grids were allowed to dry for 10 min, stained with uranyl formate, then visualised on an FEI Tecani G2 Spirit BioTwin TEM (PennState, USA) and recorded using a Gatan Orius 1000B CCD camera and Gatan Digital Micrograph software (Gatan, USA).

We have submitted all relevant data from our experiments to the EV-TRACK knowledgebase (EV-TRACK ID: EV240050) (Van Deun et al., 2017-02-28).

2.3 | Staining protocol

The concentration of unlabelled particles was measured using nFCM. Particles were diluted to 2×10^{10} particles/mL in PBS (pH 7.2, ThermoFisher, 10010023). 9 μL sample was incubated with 1 μL dye (at 10× optimal concentration, diluted in PBS), before incubation for 30 min at room temperature in the dark. The incubation concentrations of each dye are given in Table 1. Stained particles were diluted to approximately 2×10^{8} particles/mL, in TE buffer (pH 7.4, Fisher Bioreagents, BP2476-100) to a nFCM particle flow rate of between 1500 and 12,000 particles/min, then measured in triplicate.

2.4 | Antibody and membrane dye dual staining protocol

To assess the EV binding efficacy of each dye, SW620-derived EVs were dual stained with a membrane dye and a cocktail of either FITC- or APC-conjugated anti-CD9, CD63 and CD81 antibodies (Abcam—FITC CD9 (ab18241), CD63 (ab18235), CD81 (ab239256), APC CD9 (ab82389), CD81 (ab233259); Invitrogen—APC CD63 (a15712)). This followed the staining protocol described previously, but 1 μL of the antibody cocktail was added alongside the membrane dye. To allow optimal fluorescent detection (Lees et al., 2022), antibodies were diluted 30-fold (FITC) or 200-fold (APC) for incubation with EVs. Antibody optimisation data are provided in Figure S2.

2.5 | Triton ablation

To assess the proportion of membranous particles in the SW620-derived and SW480-derived EV samples, each sample was diluted to 4×10^{10} particles/mL in PBS, then diluted 2-fold with 10% Triton X-100, for a final EV concentration of 2×10^{10} particles/mL and final Triton concentration of 5%. These were incubated for 30 min at room temperature, and then measured in triplicate using nFCM.

2.6 | Dye aggregation in PBS

To assess dye aggregation, each dye was incubated with particle-free PBS, following the staining protocol described previously. The concentration of side scatter positive aggregation was calculated, using particle-free buffer as a blank. To contextualise these data, the concentrations of dye aggregates were expressed relative to 2×10^{10} particles/mL, the particle concentration utilised in staining.

2.7 | Nano-flow cytometry

A NanoAnalyzer U30 instrument (NanoFCM Inc.) equipped with dual 488/640 nm lasers was used for the simultaneous detection of side scatter (SSC) and fluorescence of individual particles. Single-photon counting avalanche photodiode detectors (SPCM APDs) with bandpass filters allowed for collection of light in specific channels (SSC - 488/10 nm; FL1—525/40 nm; FL2—670/30 nm). Gravity fed HPLC-grade water served as the sheath-fluid, sampling pressure by the air pump module was 1 kPa and measurements were taken over 60 s. Values for peak height (mean + 3 standard deviations of the background) and peak width (0.3 ms) were used as thresholds for peak identification. For each particle, peak area was recorded in all three detection channels simultaneously for use in constructing dot plots and histograms. Samples were diluted to attain a particle count within the optimal range of 1500−12,000/min. A blank measurement of TE buffer was recorded, containing 200−400 particles/min; these particles are subtracted from the sample measurement for concentration calculation.

Particle concentrations were determined by comparison to a standard containing 250 nm silica nanoparticles of known concentration. Particles were sized according to standard operating procedures using a proprietary 4-modal silica nanosphere cocktail (NanoFCM Inc., S16M-Exo). Using the NanoFCM software (NanoFCM Profession V2.0), a standard curve was generated based on the intensity of side scattered light of the four different silica particle populations of 68, 91, 113 and 155 nm in diameter. The laser was set to 15 mW and 10% SSC decay.

Data processing was handled within the nFCM Professional Suite V2.0 software, with dot plots, histograms and statistical data provided in a single PDF. Gating within the software allows for proportional analysis of subpopulations separated by fluorescent intensities.

2.8 | MFI and stain index calculation

Median fluorescence intensity (MFI) is representative of the brightness of particles stained with a given dye. MFI was defined as the median fluorescence-channel pulse area of side-scatter positive, fluorescent positive particles. To quantify brightness of stained particles, stain index was used. Stain index is calculated as the difference in MFI of the fluorescent positive and negative populations, divided by twice the standard deviation of the fluorescence intensities of the negative population (Maecker et al., 2004).

3 | RESULTS

3.1 | Defining optimal dye-to-EV ratios by dilution series

Conditioned media-derived EVs were characterised by nFCM for particles 40−200 nm diameter and tetraspanin markers (Figure S1). EVs were diluted to 2×10^{10} particles/mL and stained with a dilution series of each dye, to determine the optimum ratio of dye:EVs (Figure 1, Table 1, Figure S3). The optimum concentration of dye is high enough to saturate the EVs with dye, producing a high staining percentage and brightly labelled particles, but not so high as to leave excess dye in the buffer. Using nFCM, excess dye results in a raised fluorescence baseline, which can obscure true fluorescence signals, a phenomenon seen across multiple fluorescence platforms.

3.2 | Fluorescent detection and quantitation of labelled conditioned-media-derived EVs

A priority for efficient EV labelling is the ability to successfully bind, and make identifiable, the majority of EVs in a sample. Conditioned media-derived EVs isolated from an SW620 cell line by SEC were used to demonstrate the proportion of EVs labelled by each dye, with results varying across the panel of dyes tested (Figure 2a−g). The highest efficacy dyes were CellMask Deep Red (100%), MemGlow 640 (97.3%) and MemGlow 488 (96.4%). The lowest efficacy dyes were ExoBrite 490/515 (40.1%) and ExoBrite 640/660 (21.3%).

To test dye efficacy on EVs isolated from a different cell line, the dyes were used to stain EVs derived from an SW480 cell line (Figure 2a−g). All six dyes had binding efficacy over 50%, with MemGlow 488 (97.2%), MemGlow 640 (95.5%) and CMDR (92.4%) labelling near 100% of particles.

Both EV samples were treated with 5% Triton X-100 for 30 min to destroy membranous particles (Figure 2h). 68.6% of SW620-derived EVs were destroyed, compared to 73.4% of SW480-derived EVs.

To evaluate the false positive rate, membrane dyes were incubated in the particle-free buffer to determine the rate of dye aggregation (Figure 3). The membrane dyes tested do not form a high concentration of SSC+ (>40 nm diameter) aggregates when incubated in the buffer.

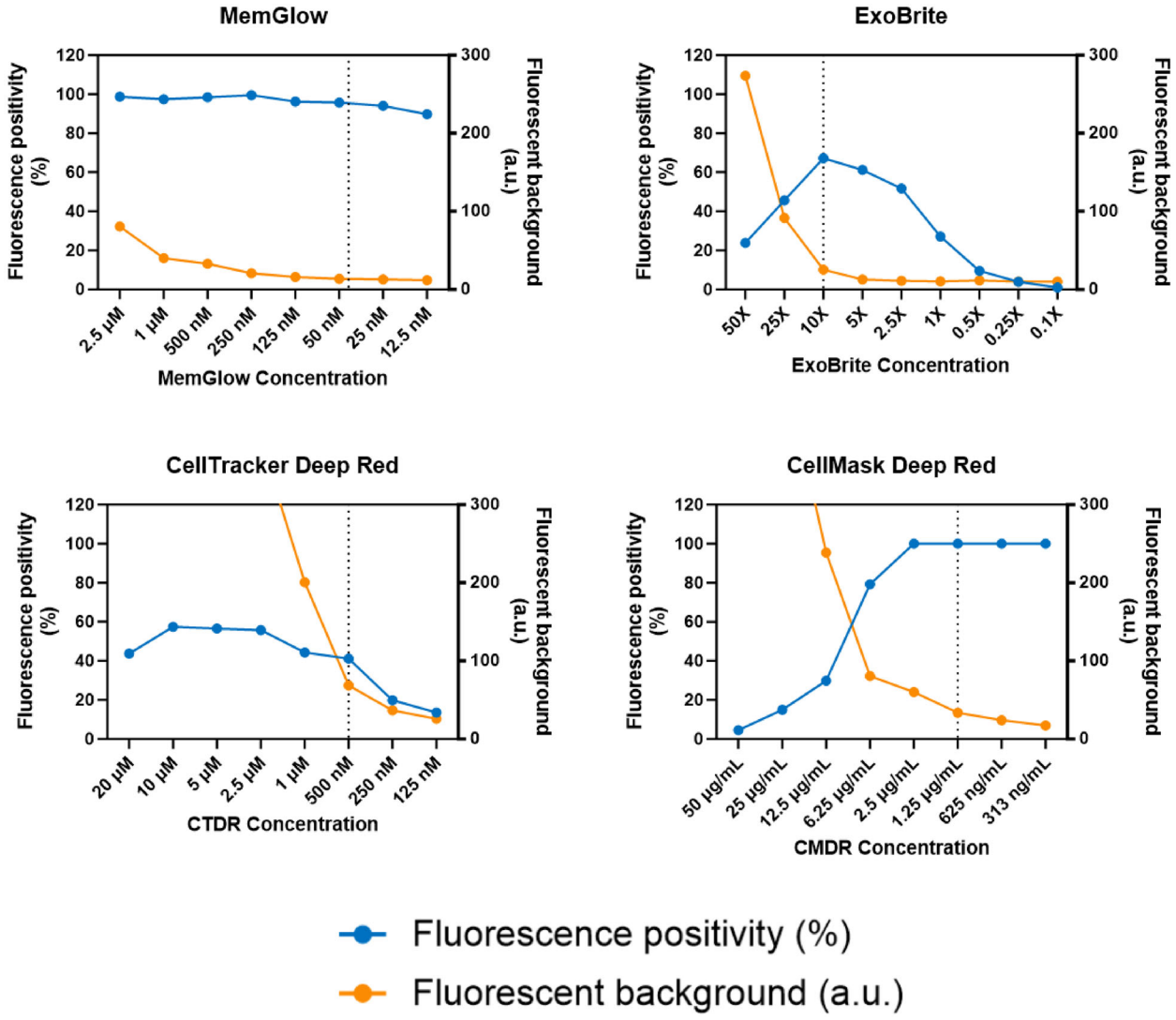

FIGURE 1 Optimisation of membrane dye staining concentration. SW480-derived extracellular vesicles (EVs) were stained with a dilution series of a panel of membrane dyes. For each dye, fluorescence positivity (blue, left y-axis) and fluorescent background (orange, right y-axis) are given for each concentration tested. The optimum concentration (dotted line) was chosen as a concentration which gives high positivity with a low background. EVs were labelled at 2×10^{10} particles/mL for all dyes.

3.3 | Co-labelling of labelled conditioned-media-derived EVs with membrane dyes and anti-tetraspanin antibodies

The dyes were used to stain SW620-derived EVs in tandem with anti-tetraspanin antibodies. Membrane staining correlated with the results of the single membrane stain.

By considering only the population of particles which were tetraspanin positive, the binding efficacy for each dye was calculated as the percentage of tetraspanin+ particles which were dye positive (Figure 4a). The highest efficacy dyes were MemGlow 640 (99.6%), CMDR (98.7%) and MemGlow 488 (97.2%). Each of the other dyes leaves tetraspanin+ EVs unstained, with the median diameter of the unstained particles being smaller than the stained particles (Figure 4b–e).

3.4 | Assessment of off-target labelling

To assess whether the membrane dyes label other lipidic structures non-specifically, purified VLDLs were purchased and stained (Figure 5a–g). VLDLs incubated with MemGlow 488 (100%) and MemGlow 640 (99.5%) appeared near 100% fluorescent positive. VLDLs stained with each of the other dyes were <15% fluorescent positive.

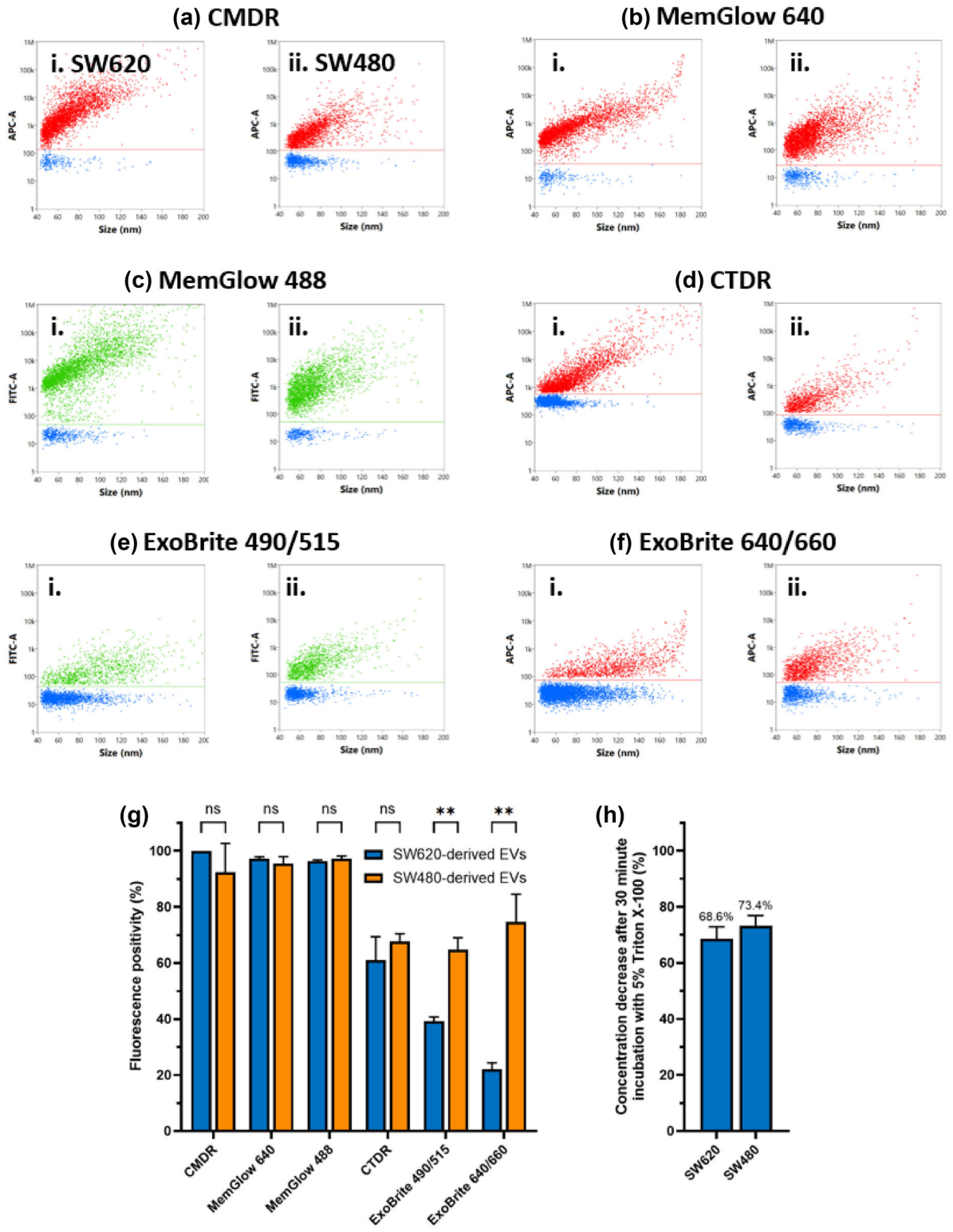

FIGURE 2 Labelling of SW620-derived and SW480-derived extracellular vesicles (EVs) with membrane dyes. (a–f) Representative bivariate dot plots of fluorescence (y-axis) against particle diameter (x-axis), showing labelling of SW620-derived (i) and SW480-derived (ii) EVs with six membrane dyes. (g) Fluorescence positivity of SW620-derived (blue) and SW480-derived (orange) EVs. Fluorescence positivity is calculated as the percentage of side-scatter positive particles which simultaneously present a fluorescence signature, as determined by the NanoFCM NanoAnalyzer ($N = 3$). ns = $p > 0.05$, *$p < 0.05$, **$p < 0.005$. (h) Percentage of particles destroyed after treatment of SW620-derived and SW480-derived EVs with 5% Triton X-100 for 30 min ($N = 3$).

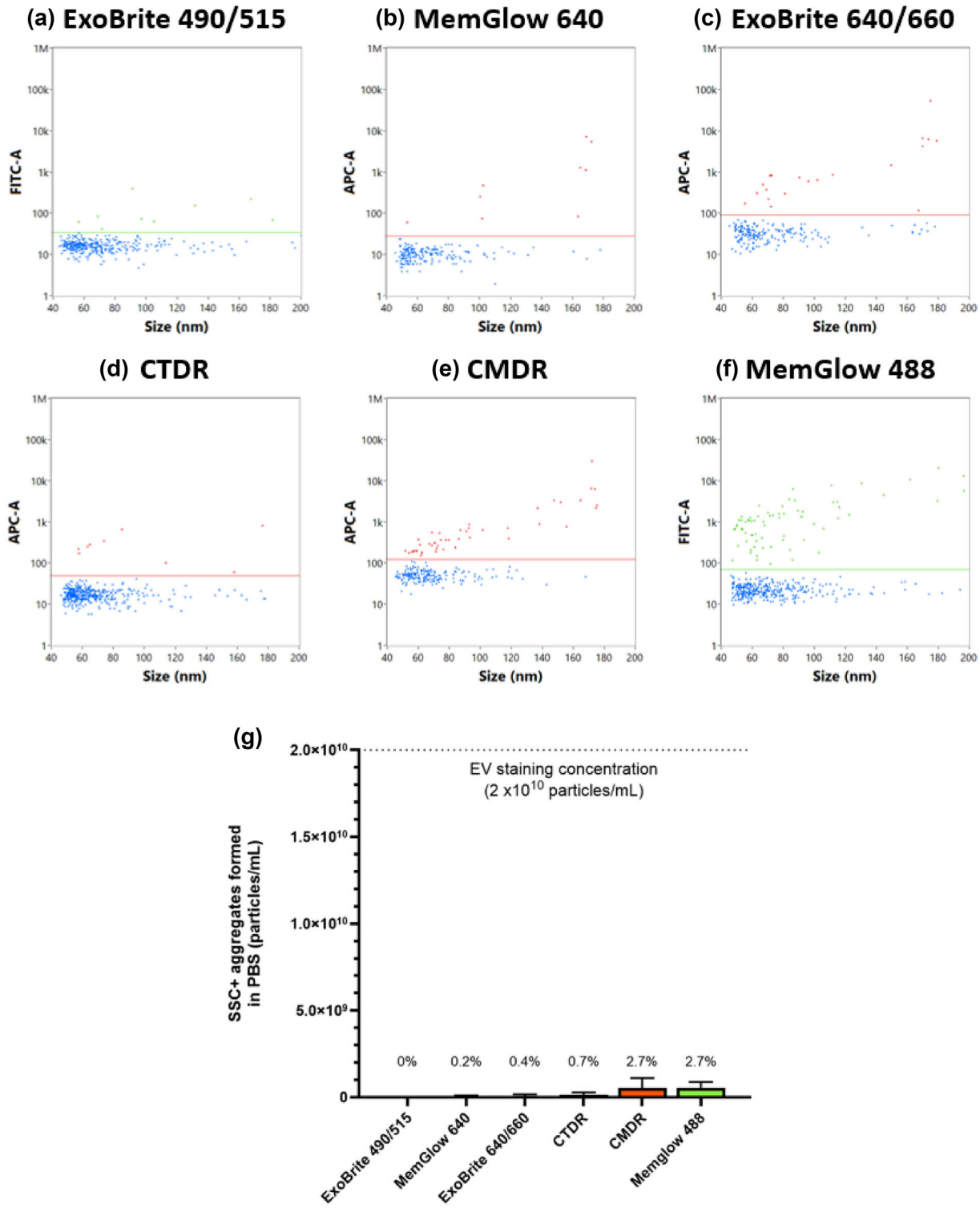

FIGURE 3 Aggregate formation after incubation of membranes dyes in particle-free PBS. (a–f) Representative bivariate dot plots of fluorescence (y-axis) against particle size (x-axis), showing aggregate formation after incubation of six membrane dyes in particle-free PBS. (g) Concentration of SSC+ aggregate formation ($N = 3$). A line is drawn at 2×10^{10} particles/mL, the standard concentration for staining, and above each bar is the percentage of aggregates relative to 2×10^{10} particles/mL.

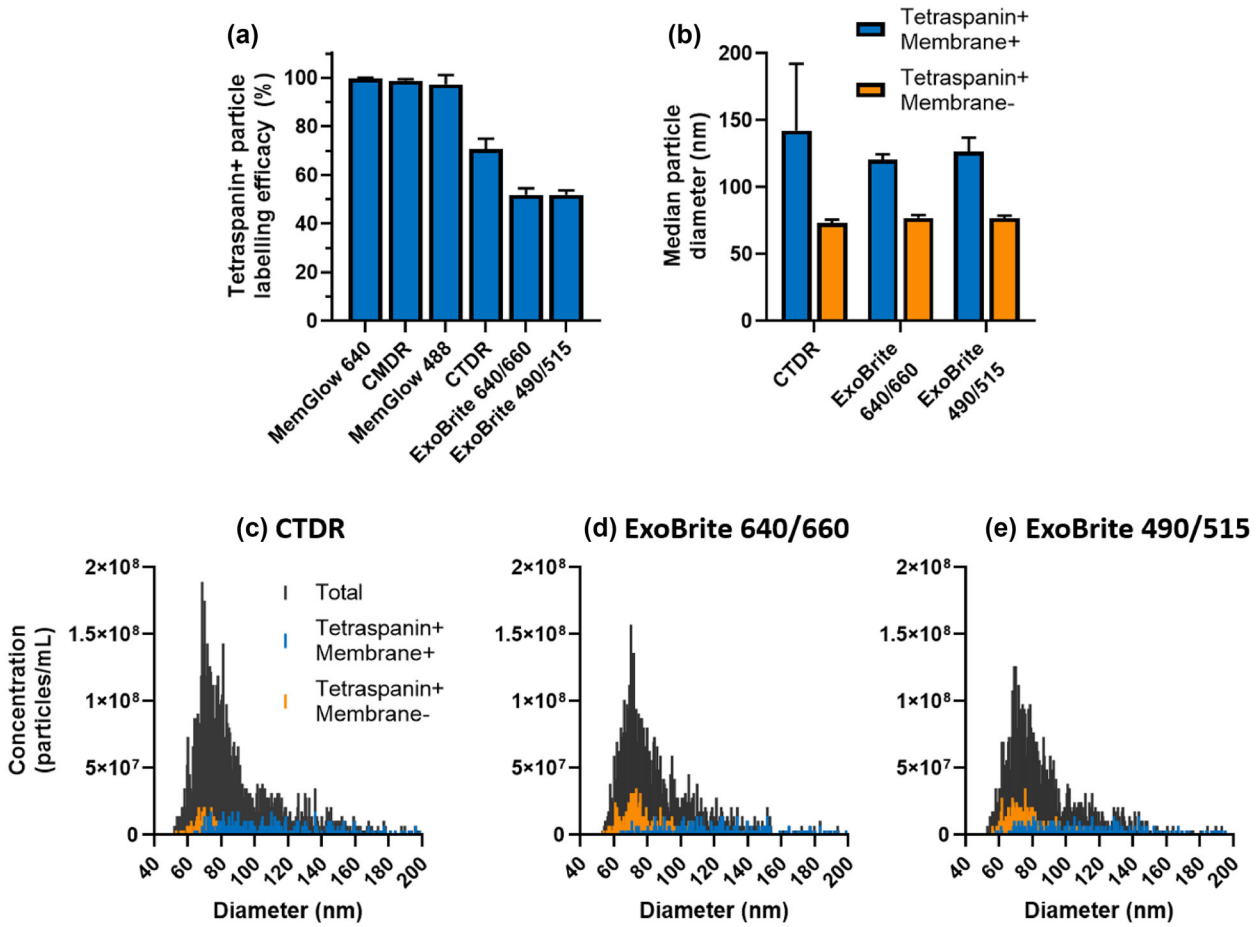

FIGURE 4 SW620-derived extracellular vesicles (EVs) dual stained with membrane dyes and a cocktail of APC- or FITC-conjugated anti-CD9, CD63 and CD81 antibodies. (a) Labelling efficacy of tetraspanin-positive SW620-derived EVs with different dyes. Labelling efficacy is calculated as the percentage of tetraspanin positive particles which were stained with each membrane dye ($N = 3$). (b) Median diameter of tetraspanin+ membrane+ (blue) and tetraspanin+ membrane- (orange) particles for each dye. (c–e) Size distribution histograms for EVs stained with each dye. Black = all particles.

To test the performance of the dyes in a more complex environment, particles were isolated from plasma using SEC. When staining these particles (Figure 5a–f,h), CMDR (100.0%), MemGlow 488 (94.0%) and MemGlow 640 (84.6%) bind a high proportion of particles. ExoBrite 640/660 (15.1%), CTDR (14.6%) and ExoBrite 490/515 (11.1%) bind a low proportion of particles.

3.5 | Dye brightness

As mentioned, the assessment of dye brightness is affected by the quantity of dye molecules incorporated into an EV, the fluorescence properties of the dye and optical properties of the analysis system. To compare the brightness of stained particles between dyes, stain index was used (Figure 6a,b). The stain index is the brightness of the stained particles relative to the fluorescent background of the sample (Maecker et al., 2004), and is commonly used in flow cytometry applications. Particles stained with MemGlow 488 had the highest stain index (242.4, Figure 6c), while particles stained with ExoBrite 490/515 (12.5, Figure 6d) and ExoBrite 640/660 (10.0) had the lowest stain indices.

3.6 | Summary

The criteria described previously were used to summarise the qualities of each dye (Table 2).

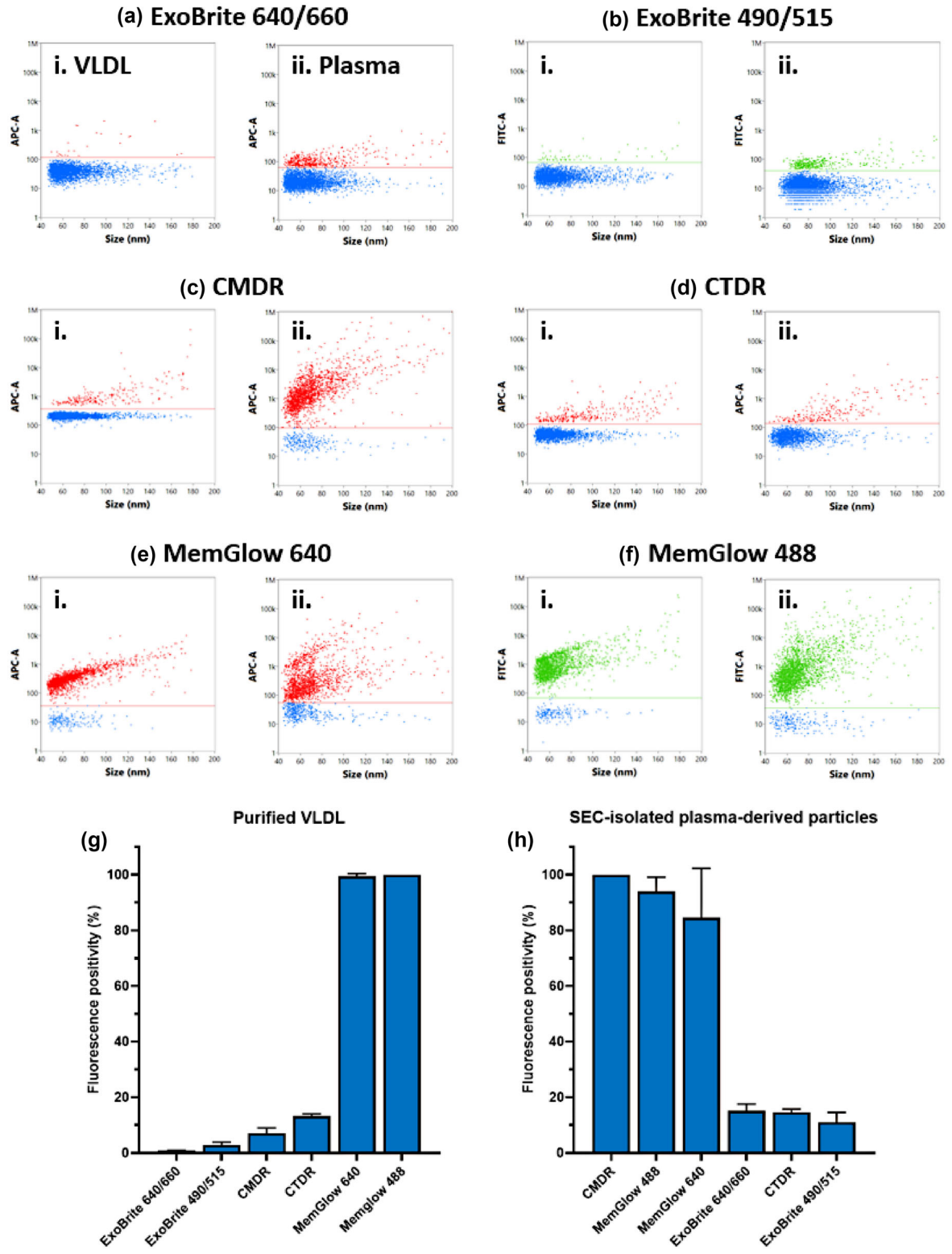

FIGURE 5 Labelling of purified VLDLs and plasma-derived particles with membrane dyes. (a–f) Representative bivariate dot plots of fluorescence (y-axis) against particle diameter (x-axis), showing labelling of purified VLDLs (i) and SEC-isolated plasma-derived particles (ii) with six membrane dyes. (g) Fluorescence positivity of stained purified VLDLs. (h) Fluorescence positivity of SEC-isolated plasma-derived particles. Fluorescence positivity is calculated as the percentage of side-scatter positive particles which simultaneously present a fluorescence signature, as determined by the NanoFCM NanoAnalyzer ($N = 3$).

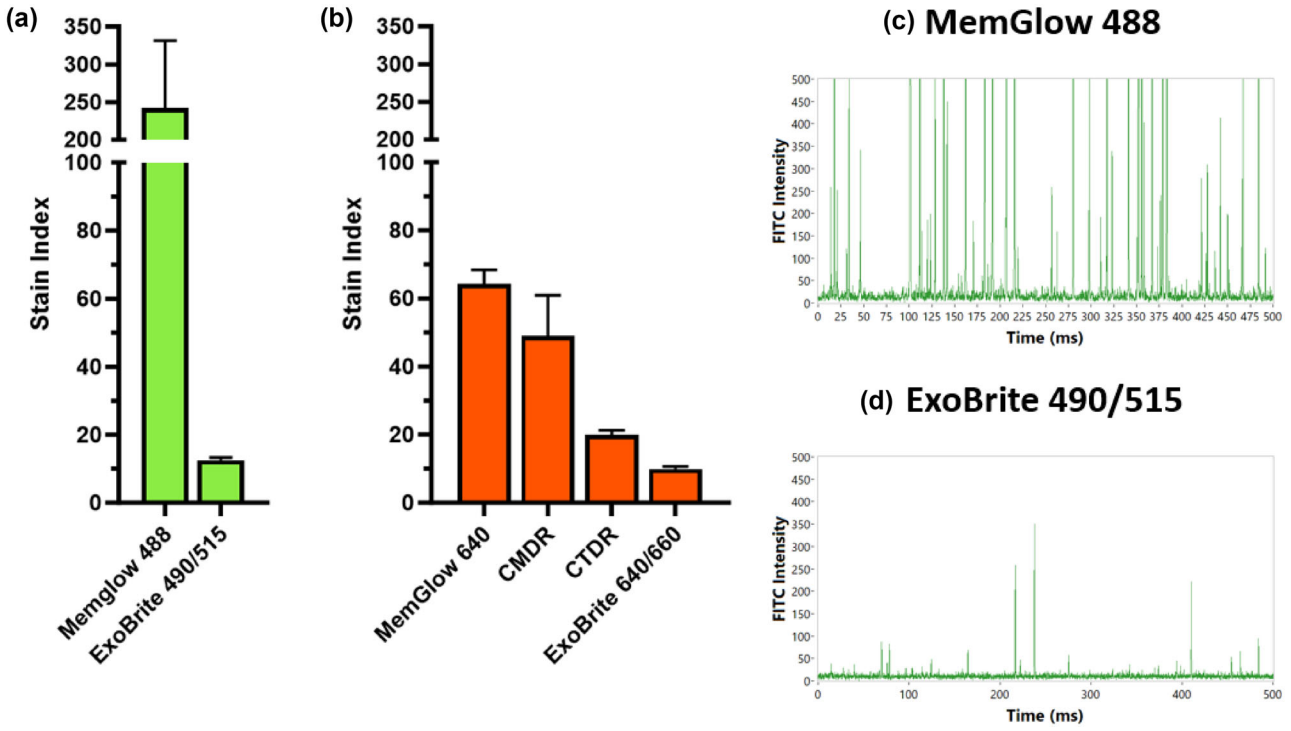

FIGURE 6 Brightness of SW620-derived extracellular vesicles (EVs) stained with six membrane dyes. (a,b) Bar charts of stain index ($N = 3$) of SW620-derived EVs stained with green (a) and red (b) membrane dyes. Median fluorescence intensity was defined as the median fluorescence-channel pulse area of side-scatter positive, fluorescent positive particles. (c,d) Representative event burst traces of SW620-derived EVs stained with MemGlow 488 (c) and ExoBrite 490/515 (d).

TABLE 2 Properties of the six investigated membrane dyes. Criteria and star ranks are defined below the table.

Dye	Efficacy[a]	Specificity[b]	Brightness[c]	Aggregation[d]
Memglow 488	***	*	***	***
MemGlow 640	***	*	***	***
ExoBrite 490/515	**	***	*	***
ExoBrite 640/660	**	***	**	***
CTDR	***	**	**	***
CMDR	***	***	**	***

[a]Efficacy is defined as the percentage of particles in an SW620-derived EV prep bound by the dye. Stars correspond to percentage positivity observed: *<20%; **20%–60%; ***>60%.
[b]Specificity is defined as the percentage of VLDLs bound by the dye. Stars correspond to percentage positivity observed: ***>10%; **10%–30%; *>30%.
[c]Brightness is defined as the stain index of labelled particles in an SW620-derived EV prep. Stars correspond to the stain index: *<10; **20–50; ***>50.
[d]Aggregation is defined as the number of side-scatter positive (SS+) particles formed when the dye is incubated without particles in its working buffer. Stars correspond to the number of SS+ particles observed: ***<200; **200–500; *>500.

4 | DISCUSSION

4.1 | Study design

Revealing good quality fluorescent labelling practices is highly important for the EV field, yet a major challenge of these types of study is the lack of starting material which can be considered 100% pure EVs (Théry et al., 2018). Whilst cell line-derived particles in the range 40–200 nm are likely to contain a majority of sEVs, other particles can be co-isolated including dsDNA, histones and vault complexes (Jeppesen et al., 2019; Liu et al., 2023). The use of secondary identifiers such as CD9/63/81 allows for the detection of EVs, which should be labelled by an effective dye so that ineffective dyes can be identified. However, these tetraspanins are known to be heterogeneously distributed throughout EV sub-populations, and variable between cell lines, biofluid sources and patients (Mizenko et al., 2021; Rydland et al., 2023). This uneven distribution was observed on EVs derived from the SW620 and SW480 cell lines used in this study (Figure S1c). As a result, 100% labelling of CM-derived particles may not be desirable, and a

pure isolation devoid of EVs is required to demonstrate the non-specific binding properties of these dyes. Purified VLDLs have been used in other studies (Botha et al., 2022) and may provide a good off-target particle to evaluate dye specificity.

To facilitate comparison between dyes, and reduce sample handling times, an early decision for the study was to maintain a simplified staining protocol in line with the protocol used for antibody staining samples for nFCM. It is possible that some dyes may perform better with different levels of handling or extra protocol steps, a consideration which is increasingly important as EV specificity requirements become more stringent.

4.2 | Best and brightest

When staining the SW620- and SW480-derived EVs, the highest efficacy dyes were CMDR, MemGlow 640 and MemGlow 488. Each of these dyes fluorescently labels over 90% of particles in both EV samples. However, treatment with 5% Triton X-100 indicates that not all particles in the EV samples are membranous (68.6% particle loss in SW620, 73.4% in SW480). This suggests that these dyes may be non-specifically labelling non-membranous particles. Each of these dyes integrates directly into the lipid bilayer, as opposed to binding membrane components (ExoBrite) or entering and relying on esterase activity (CTDR). This generic mode of action, while allowing for high-efficacy EV labelling, may also allow the dye to label non-membranous particles. Taking this into account, CTDR emerges as another promising candidate, with staining efficacy similar to Triton ablation across both EV sources (61.1% SW620, 67.6% SW480).

In addition, both ExoBrite dyes stain SW480-derived EVs with similar efficacy to Triton ablation (64.6% ExoBrite 490/515, 74.7% ExoBrite 640/660), however the staining efficacy of both with SW620-derived EVs is decreased (39.3% ExoBrite 490/515, 22.1% ExoBrite 640/660). Considering that Triton ablation is similar between the EV sources, the discrepancy between ExoBrite staining of SW620-derived and SW480-derived EVs is consistent with observations by the manufacturer that ExoBrite staining efficacy varies by cell line.

Combining the dye labelling with antibody labelling allows for a different perspective of data handling, by taking the CD9, CD63 or CD81 positive EVs and observing the proportion of these that have been successfully dye labelled. MemGlow 640, CMDR and MemGlow 488 fluorescently label near-100% of tetraspanin positive particles. However, given that each has a near-100% staining efficacy of SW620-dervied EVs as a whole, this does not indicate high specificity. On the other hand, ExoBrite 590/515 and ExoBrite 640/660 demonstrated higher proportional labelling in this defined subset (both 51.9%) than SW620-derived EVs as a whole (39.3% and 22.1%, respectively). However, both dyes leave tetraspanin positive particles unstained. Finally, CTDR also leaves tetraspanin positive particles unstained, with a labelling efficacy of 70.6%. Considering that each dye leaves tetraspanin positive particles unstained, the similarity between Triton ablation and CTDR or ExoBrite staining efficacy may be coincidental.

Considering the three dyes which leave tetraspanin+ particles unstained (CTDR, ExoBrite 640/660, ExoBrite 490/515), the median diameter of tetraspanin+ membrane+ particles is greater than that of tetraspanin+ membrane- particles (Figure 4b–e). This shows that the smaller particles within the tetraspanin positive population are not labelled with sufficient dye for detection. Smaller EVs likely express fewer copies of the GM1 ganglioside, target of the ExoBrite dyes, and contain less esterase, required for CTDR fluorescence. This leads to low fluorescence intensity, below the lower limit of detection of the NanoAnalyzer, causing the particles to be misrepresented as membrane negative.

EVs stained with MemGlow 488 are by far the brightest (Figure S4) and have the highest stain index (Figure 6a). MemGlow 488 integrates into the lipid bilayer directly (Collot et al., 2019), as opposed to targeting a specific lipid type or protein. This means that each EV can be stained with large numbers of dye molecules.

Interestingly, EVs stained with CMDR, despite having higher MFI than EVs stained with MemGlow 640 (Figure S4), had a lower stain index (Figure 6b). This is due to an elevated fluorescence background in some samples, indicating unbound CMDR molecules in the solution. The fluorescent background may be improved by post-labelling EV isolation (e.g., UC or SEC), or simply by staining with a lower concentration of CMDR. However, given the brightness of the particles, reducing the fluorescent background is not necessary to measure high staining efficacy.

None of the dyes form high concentrations of SSC+ aggregates in their staining buffer. Particles are stained at 2×10^{10} particles/mL, and each of the dyes forms $\leq 3\%$ of this many aggregates. In addition, aggregate formation is likely exaggerated in particle-free PBS, as the concentration of unbound dye is higher than that in stained particle samples. However, it must be considered that these aggregates are composed of dye molecules and are often highly fluorescent, which may lead to false positive results contributing to a small overestimation of membrane positivity.

4.3 | EV specificity

VLDLs are abundant in plasma (Johnsen et al., 2019), and their size range (~30–90 nm (German et al., 2006)) has significant overlap with that of small EVs (40–200 nm considered in this study). Therefore, VLDLs are a common co-isolate when considering SEC-isolated EVs, particularly from plasma (Koster et al., 2021).

VLDL staining shows that both MemGlow 488 and MemGlow 640 bind ~100% of VLDLs. This limits the opportunity to use MemGlow labelling for EVs in any sample where VLDL is likely to be a major co-isolate. As expected, both MemGlow 488 and 640 have high binding efficacy to SEC-isolated plasma-derived particles: 94.0% and 84.5%, respectively.

In these environments, a dye which binds 100% EVs and low percentages of VLDLs, such as CMDR (7.0% VLDL labelling), may be preferable. However, complicating this recommendation, CMDR binds 100% of SEC-isolated plasma-derived particles. These contradictory observations suggest that labelling of purified VLDLs may not be a suitable test of a dye's specificity to EVs in a complex environment, which likely contains other co-isolates, including chylomicrons (Brennan et al., 2020).

5 | CONCLUSIONS

Both MemGlow 488 and 640 are easy to use and showed bright, effective labelling of EVs. Since unbound dye self-quenches, there is a wide concentration range in which EVs are brightly stained, while the fluorescent background is low.

So far, where significant VLDL contamination is unlikely, MemGlow is a good option for EV labelling. It brightly stains near-100% of EVs, while producing a low fluorescent background, meaning there is no requirement for post-staining sample cleaning and could work on devices less sensitive than the nano-flow cytometry platform utilised here.

For workflows focused on biofluid-derived EVs, CMDR could be a viable choice as experiments staining EVs and VLDLs separately identified high efficacy and specificity.

However, as CMDR labels a high proportion of plasma-derived particles, which likely contain some non-EV particles, the specificity towards EVs needs further investigation. CMDR remains a strong choice for cell media-derived EVs, although dye removal steps should be discussed to reduce background noise and increase stain index.

Together, these dyes cover a range of applications for EV labelling, and could be applicable for future EV research. This study highlights the need for thorough optimisation and characterisation of dyes prior to use.

5.1 | Future work

While this study answers many initial questions surrounding the use of membrane dyes for fluorescent EV detection, much work remains to be done. Most importantly, the panel of dyes needs to be expanded to encompass a wider range of available dyes. Other parameters should be investigated, including the leeching of dyes from stained to unstained particles and the fluorescent bleaching qualities of the fluorophores. The methods to identify off-target labelling of co-isolates or contaminates in EV isolations need further refinement and qualification of dyes working across multiple measurement techniques and instruments will greatly benefit the EV field.

In the future, we will continue to test commercially available and novel dyes, to identify those suitable for different EV applications, such as cell culture or biofluid work and provide insight and guidance for EV work-flows.

AUTHOR CONTRIBUTIONS

Joseph Brealey: Data curation (equal); formal analysis (equal); investigation (equal); writing—original draft (equal); writing—review and editing (equal). **Rebecca lees**: Data curation (equal); formal analysis (equal); investigation (equal). **Robert Tempest**: Investigation (equal); writing—review and editing (equal). **Alice Law**: Writing—review and editing (equal). **Sonia Guarnerio**: Investigation (equal); resources (equal); writing—review and editing (equal). **Rawan Maani**: Data curation (equal); formal analysis (equal); investigation (equal). **Soozana Puvanenthiran**: Investigation (equal); resources (equal). **Nick Peake**: Resources (equal); writing—review and editing (equal). **Ryan Pink**: Resources (equal); writing—review and editing (equal). **Ben Peacock**: Conceptualization (equal); investigation (equal); methodology (equal); project administration (equal); writing—original draft (equal); writing—review and editing (equal).

ACKNOWLEDGMENT

The authors have nothing to report.

CONFLICT OF INTEREST STATEMENT

J.B. and B.P. are employees of NanoFCM Co., Ltd. and their contributions to this manuscript were made as part of their employment. R.L., R.T. and A.L. were employees of NanoFCM Co., Ltd. and their contributions to this manuscript were made as part of their employment.

DATA AVAILABILITY STATEMENT

PDF summaries of the data that support the findings of this study are available on FigShare (https://figshare.com/projects/Shining_a_Light_on_Fluorescent_EV_Dyes_Evaluating_Efficacy_Specificity_and_Suitability_by_Nano-Flow_Cytometry/205753). Other data are available from the corresponding author, B.P., upon reasonable request.

ORCID

Joseph Brealey https://orcid.org/0000-0002-3013-9375
Rebecca Lees https://orcid.org/0000-0001-5682-2642
Ryan Pink https://orcid.org/0000-0001-7501-558X
Ben Peacock https://orcid.org/0000-0002-7823-8719

REFERENCES

Baldauf, K. J., Royal, J. M., Hamorsky, K. T., & Matoba, N. (2015). Cholera toxin B: One subunit with many pharmaceutical applications. *Toxins*, *7*(3), 974–996. https://doi.org/10.3390/toxins7030974

Banks, H. T., Choi, A., Huffman, T., Nardini, J., Poag, L., & Thompson, W. C. (2013). Quantifying CFSE label decay in flow cytometry data. *Applied Mathematics Letters*, *26*(5), 571–577. https://doi.org/10.1016/j.aml.2012.12.010

Bağcı, C., Sever-Bahcekapili, M., Belder, N., Bennett, A. P. S., Erdener, Ş. E., & Dalkara, T. (2022). Overview of extracellular vesicle characterization techniques and introduction to combined reflectance and fluorescence confocal microscopy to distinguish extracellular vesicle subpopulations. *Neurophotonics*, *9*(02), 021903. https://doi.org/10.1117/1.nph.9.2.021903

Botha, J., Handberg, A., & Simonsen, J. B. (2022). Lipid-based strategies used to identify extracellular vesicles in flow cytometry can be confounded by lipoproteins: Evaluations of annexin V, lactadherin, and detergent lysis. *Journal of Extracellular Vesicles*, *11*(4), e12200. https://doi.org/10.1002/jev2.12200

Brennan, K., Martin, K., FitzGerald, S. P., O'Sullivan, J., Wu, Y., Blanco, A., Richardson, C., & Mc Gee, M. M. (2020). A comparison of methods for the isolation and separation of extracellular vesicles from protein and lipid particles in human serum. *Scientific Reports*, *10*(1), 1039. https://doi.org/10.1038/s41598-020-57497-7

Buzas, E. I. (2023). The roles of extracellular vesicles in the immune system. *Nature Reviews Immunology*, *23*(4), 236–250. https://doi.org/10.1038/s41577-022-00763-8

Chang, W. H., Cerione, R. A., & Antonyak, M. A. (2021). Extracellular Vesicles and Their Roles in Cancer Progression. *Methods in Molecular Biology*, *2174*, 143–170. https://doi.org/10.1007/978-1-0716-0759-6_10

Chen, C., Cai, N., Niu, Q., Tian, Y., Hu, Y., & Yan, X. (2023). Quantitative assessment of lipophilic membrane dye-based labelling of extracellular vesicles by nano-flow cytometry. *J Extracell Vesicles*, *12*(8), e12351. https://doi.org/10.1002/jev2.12351

Chuo, S. T.-Y., Chien, J. C.-Y., & Lai, C. P.-K. (2018). Imaging extracellular vesicles: Current and emerging methods. *Journal of Biomedical Science*, *25*(1), 91. https://doi.org/10.1186/s12929-018-0494-5

Collot, M., Ashokkumar, P., Anton, H., Boutant, E., Faklaris, O., Galli, T., Mély, Y., Danglot, L., & Klymchenko, A. S. (2019). MemBright: A family of fluorescent membrane probes for advanced cellular imaging and neuroscience. *Cell Chemical Biology*, *26*(4), 600–614. e7. https://doi.org/10.1016/j.chembiol.2019.01.009

Colombo, F., Norton, E. G., & Cocucci, E. (2021). Microscopy approaches to study extracellular vesicles. *Biochimica Et Biophysica Acta. General Subjects*, *1865*(4), 129752. https://doi.org/10.1016/j.bbagen.2020.129752

Contreras, H., Alarcón-Zapata, P., Nova-Lamperti, E., Ormazabal, V., Varas-Godoy, M., Salomon, C., & Zuniga, F. A. (2023). Comparative study of size exclusion chromatography for isolation of small extracellular vesicle from cell-conditioned media, plasma, urine, and saliva [Original Research]. *Frontiers in Nanotechnology*, *5*, 1146772. https://doi.org/10.3389/fnano.2023.1146772

Couch, Y., Buzàs, E. I., Di Vizio, D., Gho, Y. S., Harrison, P., Hill, A. F., Lötvall, J., Raposo, G., Stahl, P. D., Théry, C., Witwer, K. W., & Carter, D. R. F. (2021). A brief history of nearly EV-erything—The rise and rise of extracellular vesicles. *Journal of Extracellular Vesicles*, *10*(14), e12144. https://doi.org/10.1002/jev2.12144

De Sousa, K. P., Rossi, I., Abdullahi, M., Ramirez, M. I., Stratton, D., & Inal, J. M. (2023). Isolation and characterization of extracellular vesicles and future directions in diagnosis and therapy. *Wiley Interdisciplinary Reviews. Nanomedicine and Nanobiotechnology*, *15*(1), e1835. https://doi.org/10.1002/wnan.1835

Dehghani, M., & Gaborski, T. R. (2020). Chapter two—fluorescent labeling of extracellular vesicles. In S. Spada & L. Galluzzi (Eds.), *Methods in Enzymology* (Vol. 645, pp. 15–42). Academic Press. https://doi.org/10.1016/bs.mie.2020.09.002

Durak-Kozica, M., Baster, Z., Kubat, K., & Stępień, E. (2018). 3D visualization of extracellular vesicle uptake by endothelial cells. *Cellular & Molecular Biology Letters*, *23*(1), 57. https://doi.org/10.1186/s11658-018-0123-z

Fan, Y., Pionneau, C., Cocozza, F., Boëlle, P. Y., Chardonnet, S., Charrin, S., Théry, C., Zimmermann, P., & Rubinstein, E. (2023). Differential proteomics argues against a general role for CD9, CD81 or CD63 in the sorting of proteins into extracellular vesicles. *Journal of Extracellular Vesicles*, *12*(8), e12352. https://doi.org/10.1002/jev2.12352

German, J. B., Smilowitz, J. T., & Zivkovic, A. M. (2006). Lipoproteins: When size really matters. *Current Opinion in Colloid & Interface Science*, *11*(2-3), 171–183. https://doi.org/10.1016/j.cocis.2005.11.006

Gurunathan, S., Kang, M.-H., & Kim, J.-H. (2021). A comprehensive review on factors influences biogenesis, functions, therapeutic and clinical implications of exosomes. *International Journal of Nanomedicine*, *16*, 1281–1312. https://doi.org/10.2147/ijn.s291956

Jeppesen, D. K., Fenix, A. M., Franklin, J. L., Higginbotham, J. N., Zhang, Q., Zimmerman, L. J., Liebler, D. C., Ping, J., Liu, Q., Evans, R., Fissell, W. H., Patton, J. G., Rome, L. H., Burnette, D. T., & Coffey, R. J. (2019). Reassessment of exosome composition. *Cell*, *177*(2), 428–445. e18. https://doi.org/10.1016/j.cell.2019.02.029

Johnsen, K. B., Gudbergsson, J. M., Andresen, T. L., & Simonsen, J. B. (2019). What is the blood concentration of extracellular vesicles? Implications for the use of extracellular vesicles as blood-borne biomarkers of cancer. *Biochimica Et Biophysica Acta (BBA)—Reviews on Cancer*, *1871*(1), 109–116. https://doi.org/10.1016/j.bbcan.2018.11.006

Kalluri, R., & LeBleu, V. S. (2020). The biology. *Science*, *367*(6478), eaau6977. https://doi.org/10.1126/science.aau6977

Kornilov, R., Puhka, M., Mannerström, B., Hiidenmaa, H., Peltoniemi, H., Siljander, P., Seppänen-Kaijansinkko, R., & Kaur, S. (2018). Efficient ultrafiltration-based protocol to deplete extracellular vesicles from fetal bovine serum. *Journal of Extracellular Vesicles*, *7*(1), 1422674. https://doi.org/10.1080/20013078.2017.1422674

Koster, H. J., Rojalin, T., Powell, A., Pham, D., Mizenko, R. R., Birkeland, A. C., & Carney, R. P. (2021). Surface enhanced Raman scattering of extracellular vesicles for cancer diagnostics despite isolation dependent lipoprotein contamination. *Nanoscale*, *13*(35), 14760–14776. https://doi.org/10.1039/d1nr03334d

Kowal, J., Arras, G., Colombo, M., Jouve, M., Morath, J. P., Primdal-Bengtson, B., Dingli, F., Loew, D., Tkach, M., & Théry, C. (2016). Proteomic comparison defines novel markers to characterize heterogeneous populations of extracellular vesicle subtypes. *Proceedings of the National Academy of Sciences of the United States of America*, *113*(8), E968–E977. https://doi.org/10.1073/pnas.1521230113

Kwon, Y., & Park, J. (2022). Methods to analyze extracellular vesicles at single particle level. *Micro and Nano Systems Letters*, *10*(1), https://doi.org/10.1186/s40486-022-00156-5

Lai, C. P., Kim, E. Y., Badr, C. E., Weissleder, R., Mempel, T. R., Tannous, B. A., & Breakefield, X. O. (2015). Visualization and tracking of tumour extracellular vesicle delivery and RNA translation using multiplexed reporters. *Nature Communications*, *6*(1), 7029. https://doi.org/10.1038/ncomms8029

Laulagnier, K., Javalet, C., Hemming, F. J., Chivet, M., Lachenal, G., Blot, B., Chatellard, C., & Sadoul, R. (2018). Amyloid precursor protein products concentrate in a subset of exosomes specifically endocytosed by neurons. *Cellular and Molecular Life Sciences: CMLS*, *75*(4), 757–773. https://doi.org/10.1007/s00018-017-2664-0

Lees, R., Tempest, R., Law, A., Aubert, D., Davies, O. G., Williams, S., Peake, N., & Peacock, B. (2022). Single extracellular vesicle transmembrane protein characterization by nano-flow cytometry. *Journal of Visualized Experiments: JoVE*, e64020. https://doi.org/10.3791/64020

Liu, X., Nizamudeen, Z., Hill, C. J., Parmenter, C., Arkill, K. P., Lambert, D. W., & Hunt, S. (2023). *Vault Particles are Common Contaminants of Extracellular Vesicle Preparations*. Cold Spring Harbor Laboratory.

Maecker, H. T., Frey, T., Nomura, L. E., & Trotter, J. (2004). Selecting fluorochrome conjugates for maximum sensitivity. *Cytometry Part A*, *62A*(2), 169–173. https://doi.org/10.1002/cyto.a.20092

Matsui, T., Osaki, F., Hiragi, S., Sakamaki, Y., & Fukuda, M. (2021). ALIX and ceramide differentially control polarized small extracellular vesicle release from epithelial cells. *EMBO Reports*, *22*(5), e51475. https://doi.org/10.15252/embr.202051475

Melling, G. E., Conlon, R., Pantazi, P., Dellar, E. R., Samuel, P., Baena-Lopez, L. A., Simpson, J. C., & Carter, D. R. F. (2022). Confocal microscopy analysis reveals that only a small proportion of extracellular vesicles are successfully labelled with commonly utilised staining methods. *Scientific Reports*, *12*(1), 262. https://doi.org/10.1038/s41598-021-04225-4

Mizenko, R. R., Brostoff, T., Rojalin, T., Koster, H. J., Swindell, H. S., Leiserowitz, G. S., Wang, A., & Carney, R. P. (2021). Tetraspanins are unevenly distributed across single extracellular vesicles and bias sensitivity to multiplexed cancer biomarkers. *Journal of Nanobiotechnology*, *19*(1), 250. https://doi.org/10.1186/s12951-021-00987-1

Pužar Dominkuš, P., Stenovec, M., Sitar, S., Lasič, E., Zorec, R., Plemenitaš, A., Žagar, E., Kreft, M., & Lenassi, M. (2018). PKH26 labeling of extracellular vesicles: Characterization and cellular internalization of contaminating PKH26 nanoparticles. *Biochimica Et Biophysica Acta. Biomembranes*, *1860*(6), 1350–1361. https://doi.org/10.1016/j.bbamem.2018.03.013

Quah, B. J. C., & Parish, C. R. (2010). The use of carboxyfluorescein diacetate succinimidyl ester (CFSE) to monitor lymphocyte proliferation. *Journal of Visualized Experiments*, e2259. https://doi.org/10.3791/2259

Rydland, A., Heinicke, F., Flåm, S. T., Mjaavatten, M. D., & Lie, B. A. (2023). Small extracellular vesicles have distinct CD81 and CD9 tetraspanin expression profiles in plasma from rheumatoid arthritis patients. *Clinical and Experimental Medicine*, *23*(6), 2867–2875. https://doi.org/10.1007/s10238-023-01024-1

Sun, W., Li, Z., Zhou, X., Yang, G., & Yuan, L. (2019). Efficient exosome delivery in refractory tissues assisted by ultrasound-targeted microbubble destruction. *Drug Delivery*, *26*(1), 45–50. https://doi.org/10.1080/10717544.2018.1534898

Théry, C., Witwer, K. W., Aikawa, E., Alcaraz, M. J., Anderson, J. D., Andriantsitohaina, R., Antoniou, A., Arab, T., Archer, F., Atkin-Smith, G. K., Ayre, D. C., Bach, J. M., Bachurski, D., Baharvand, H., Balaj, L., Baldacchino, S., Bauer, N. N., Baxter, A. A., Bebawy, M., … Zuba-Surma, E. K. (2018). Minimal information for studies of extracellular vesicles 2018 (MISEV2018): A position statement of the International Society for Extracellular Vesicles and update of the MISEV2014 guidelines. *Journal of Extracellular Vesicles*, *7*(1), 1535750. https://doi.org/10.1080/20013078.2018.1535750

Tian, Y., Ma, L., Gong, M., Su, G., Zhu, S., Zhang, W., Wang, S., Li, Z., Chen, C., Li, L., Wu, L., & Yan, X. (2018). Protein profiling and sizing of extracellular vesicles from colorectal cancer patients via flow cytometry. *ACS Nano*, *12*(1), 671–680. https://doi.org/10.1021/acsnano.7b07782

Tognoli, M. L., Dancourt, J., Bonsergent, E., Palmulli, R., de Jong, O. G., Van Niel, G., Rubinstein, E., Vader, P., & Lavieu, G. (2023). Lack of involvement of CD63 and CD9 tetraspanins in the extracellular vesicle content delivery process. *Communications Biology*, *6*(1), 532. https://doi.org/10.1038/s42003-023-04911-1

Van Deun, J., Mestdagh, P., Agostinis, P., Akay, Ö., Anand, S., Anckaert, J., Martinez, Z. A., Baetens, T., Beghein, E., Bertier, L., Berx, G., Boere, J., Boukouris, S., Bremer, M., Buschmann, D., Byrd, J. B., Casert, C., Cheng, L., Cmoch, A., … Hendrix, A. (2017). EV-TRACK: Transparent reporting and centralizing knowledge in extracellular vesicle research. *Nature Methods*, *14*(3), 228–232. https://doi.org/10.1038/nmeth.4185

Yates, A. G., Pink, R. C., Erdbrügger, U., Siljander, P. R., Dellar, E. R., Pantazi, P., Akbar, N., Cooke, W. R., Vatish, M., Dias-Neto, E., Anthony, D. C., & Couch, Y. (2022). In sickness and in health: The functional role of extracellular vesicles in physiology and pathology in vivo: Part I: Health and Normal Physiology: Part I: Health and Normal Physiology. *Journal of Extracellular Vesicles*, *11*(1), e12151. https://doi.org/10.1002/jev2.12151

Zhu, S., Ma, L., Wang, S., Chen, C., Zhang, W., Yang, L., Hang, W., Nolan, J. P., Wu, L., & Yan, X. (2014). Light-scattering detection below the level of single fluorescent molecules for high-resolution characterization of functional nanoparticles. *ACS Nano*, *8*(10), 10998–11006. https://doi.org/10.1021/nn505162u

SUPPORTING INFORMATION

Additional supporting information can be found online in the Supporting Information section at the end of this article.

How to cite this article: Brealey, J., Lees, R., Tempest, R., Law, A., Guarnerio, S., Maani, R., Puvanenthiran, S., Peake, N., Pink, R., & Peacock, B. (2024). Shining a light on fluorescent EV dyes: Evaluating efficacy, specificity and suitability by nano-flow cytometry. *Journal of Extracellular Biology*, *3*, e70006. https://doi.org/10.1002/jex2.70006